Dark photon production through positron annihilation in beam-dump experiments

L. Marsicano,[1,2] M. Battaglieri,[1] M. Bondí,[3] C. D. R. Carvajal,[4] A. Celentano,[1]
M. De Napoli,[3] R. De Vita,[1] E. Nardi,[5] M. Raggi,[6] and P. Valente[7]

[1]*Istituto Nazionale di Fisica Nucleare, Sezione di Genova, 16146 Genova, Italy*
[2]*Universitá degli studi di Genova, 16126 Genova, Italy*
[3]*Istituto Nazionale di Fisica Nucleare, Sezione di Catania, 95125 Catania, Italy*
[4]*Universidad de Antioquia, Instituto de Física, Calle 70 No. 52-21, Medellín, Colombia*
[5]*Istituto Nazionale di Fisica Nucleare, Laboratori Nazionali di Frascati, C.P. 13, 00044 Frascati, Italy*
[6]*Universitá degli studi Roma La Sapienza, 00185 Roma, Italy*
[7]*Istituto Nazionale di Fisica Nucleare, Sezione di Roma, 00185 Roma, Italy*

High-energy positron annihilation is a viable mechanism to produce dark photons (A'). This reaction plays a significant role in beam-dump experiments using multi-GeV electron beams on thick targets by enhancing the sensitivity to A' production. The positrons produced by the electromagnetic shower can produce an A' via nonresonant ($e^+ + e^- \to \gamma + A'$) and resonant ($e^+ + e^- \to A'$) annihilation on atomic electrons. For visible decays, the contribution of resonant annihilation results in a larger sensitivity with respect to limits derived by the commonly used A'-strahlung in certain kinematic regions. When included in the evaluation of the E137 beam-dump experiment reach, positron annihilation pushes the current limit on ε downwards by a factor of 2 in the range 33 MeV/c^2 < $m_{A'}$ < 120 MeV/c^2.

I. MOTIVATIONS

Fitting dark matter (DM) in the Standard Model (SM) of elementary particles is one of the most prominent open questions of contemporary physics. Null results in the direct detection of halo DM calls for alternative explanations to the current weakly interacting massive particle paradigm [1]. One of them conjectures the existence of a new class of lighter elementary particles not charged under the SM strong, weak, or electromagnetic forces. A well-motivated scenario considers DM with a mass below 1 GeV/c^2, charged under a new $U(1)_D$ gauge symmetry, that interacts with the SM particles via the exchange of a light spin-1 boson (a heavy photon or A', also called a dark photon). The coupling between SM particles and dark photons is induced by the kinetic mixing operator. This mechanism, originally suggested by Holdom [2] as a possible minimal extension of the SM, has been lately interpreted as a portal between the SM world and a new dark sector [3,4]. The low-energy effective Lagrangian extending the SM to include dark photons can be written as follows:

$$\mathcal{L}_{\text{eff}} = \mathcal{L}_{\text{SM}} - \frac{1}{4} F'_{\mu\nu} F'^{\mu\nu} + \frac{1}{2} m^2_{A'} A'_\mu A'^\mu - \frac{\varepsilon}{2} F'_{\mu\nu} F^{\mu\nu}, \quad (1)$$

where $F'_{\mu\nu}$ is the field strength of the hidden gauge field A'_μ, $m_{A'}$ the mass of the heavy photon, and $F_{\mu\nu}$ the SM photon field strength. The kinetic mixing parameter ε is expected to be small, in the range of $\sim 10^{-4}$–10^{-2} ($\sim 10^{-6}$–10^{-3}) if the mixing is generated by one- (two-) loop interaction [2,5–7]. Depending on the relative mass of the A' and the DM particles, the A' can decay to SM particles (visible decay) or to light DM states (invisible decay).

This new idea generated many theoretical and phenomenological studies [3,4,8–14], stimulated the reanalysis and interpretation of old data [15–20], and promoted new experimental programs, searching both for the A' [21–28] and for light DM states [29–34]. For a comprehensive review of the subject, we refer the reader to Refs. [35,36].

In this context, accelerator-based experiments that make use of an intense electron beam of moderate energy (~ 10 GeV) dumped on a thick target (beam dump) are sensitive to a wide area of ε vs $m_{A'}$ parameter space [10,37]. Figure 1 shows limits in (ε vs $m_{A'}$) extracted from the reanalysis of past electron beam-dump experiment data [38–42], assuming the A' decays visibly [37,43]. Even if, in principle, the concept is the same, the limited intensity prevented so far running beam-dump experiments that use a primary positron beam. In this paper, we show that
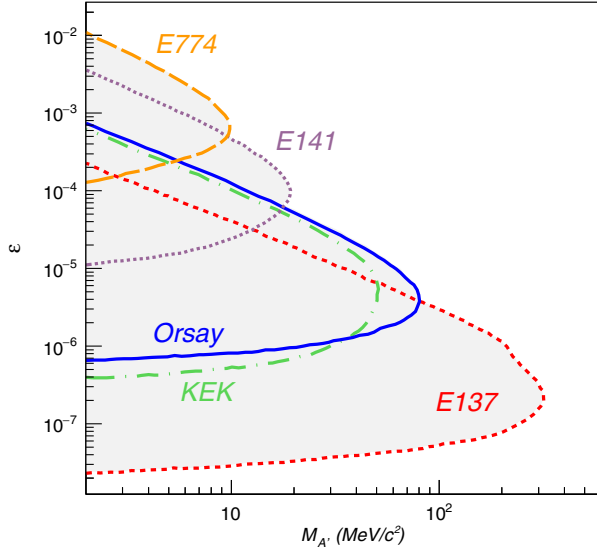
FIG. 1.   Limits on coupling ε vs A' mass resulting from null results reported in beam-dump experiments, assuming dark photons decay visibly. Curves report limits derived in Ref. [37].

positrons play an important role also in electron beam-dump experiments, where they are copiously produced in the electromagnetic shower developing in the thick target. When the sizable contribution of secondary positron annihilations via nonresonant and resonant production is considered, exclusion limits are pushed downwards in certain kinematics regions, improving the experimental sensitivity of electron beam-dump experiments.

The paper is organized as follows. In Sec. II, we briefly discuss the A' production mechanism by $O(\text{GeV})$ positrons impinging on a fixed target. In Sec. III, we focus on the electron-beam thick-target case. After reviewing the main features of positron production in an electron-induced electromagnetic shower, we discuss the effect of the resulting e^+ angular and energy distribution on A' production in the dump and its detection in a distant detector. Finally, Sec. IV presents the application of this new approach to the E137 experiment [39], the electron-beam fixed target effort that placed the most stringent exclusion limits in the A' parameter space.

II. A' PRODUCTION BY POSITRONS

The processes involved in dark photon production by $O(\text{GeV})$ positrons are shown in Fig. 2. Diagrams (a) and (b) describe, respectively, the A' production through resonant ($e^+ + e^- \rightarrow A'$) and nonresonant ($e^+ + e^- \rightarrow \gamma + A'$) positron annihilation on atomic electrons. The first production mechanism was recently put forth [44,45] as a powerful tool to test at the forthcoming Positron annihilation into dark matter experiment (PADME) experiment [25] hints of a 17 MeV A' from anomalous e^+e^- production in ^{8}Be nuclear transitions [46]. Diagram (c), instead, represents the "A'-strahlung" process, i.e., the radiative A' emission by an impinging e^+ in the EM field of a target
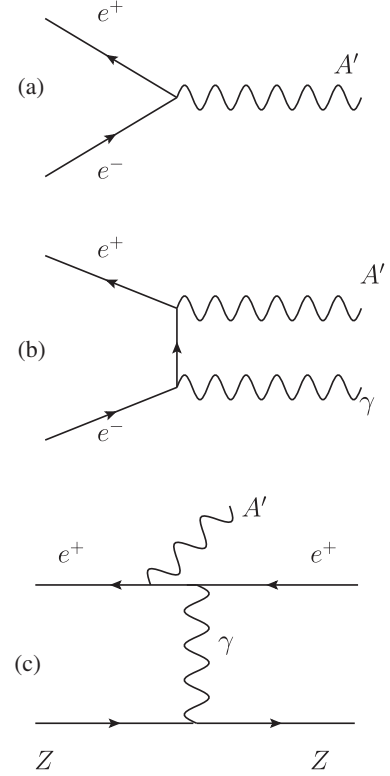

FIG. 2.   Three different A' production mechanisms by high-energy positrons on a fixed target: (a) resonant A' production in e^+e^- annihilation; (b) A'-strahlung in e^+e^- annihilation; (c) A'-strahlung in e^+-nucleus scattering.

nucleus. At first order, the corresponding cross section is the same as the one for the equivalent e^- process [47].

The cross sections for the annihilation processes scale as $\varepsilon^2\alpha$ (resonant) and $\varepsilon^2\alpha^2$ (nonresonant), where α is the electromagnetic fine-structure constant, compared to the $\varepsilon^2\alpha^3$ dependence characteristics of the A'-strahlung diagram. Specifically, the resonant diagram in Fig. 2(a) yields the total cross section:

$$\sigma_r = \sigma_{\text{peak}} \frac{\Gamma_{A'}^2/4}{(\sqrt{s} - m_{A'})^2 + \Gamma_{A'}^2/4}, \qquad (2)$$

where m_e is the electron mass, s is the e^+e^- system invariant mass squared, $\sigma_{\text{peak}} = 12\pi/m_{A'}^2$ is the resonant cross section at the peak, and $\Gamma_{A'} = \frac{1}{3}m_{A'}\varepsilon^2\alpha$ is the A' decay width in the limit $m_e/m_{A'} \rightarrow 0$. Given that $\Gamma_{A'}/m_{A'} \ll 1$ if $\varepsilon \ll 1$, for the resonant case the narrow-width approximation [48] has been consistently used. The differential and total cross sections for the nonresonant diagram in Fig. 2(b) read

$$\frac{d\sigma}{dz} = \frac{4\pi\varepsilon^2\alpha^2}{s}\left(\frac{s - m_{A'}^2}{2s}\frac{1 + z^2}{1 - \beta^2 z^2} + \frac{2m_{A'}^2}{s - m_{A'}^2}\frac{1}{1 - \beta^2 z^2}\right), \quad (3)$$

$$\sigma_{\text{nr}} = \frac{8\pi\alpha^2\varepsilon^2}{s}\left[\left(\frac{s - m_{A'}^2}{2s} + \frac{m_{A'}^2}{s - m_{A'}^2}\right)\log\frac{s}{m_e^2} - \frac{s - m_{A'}^2}{2s}\right], \quad (4)$$

with z being the cosine of the A' emission angle in the e^+e^- rest frame, measured with respect to the positron axis, and $\beta = \sqrt{1 - \frac{4m_e^2}{s}}$. It is worth mentioning that these results were derived at the tree level, keeping the leading m_e dependence to avoid nonphysical divergences when $|z| \to 1$ [26]. To avoid infrared divergences when $s \to m_{A'}^2$, we applied a low-energy cutoff for the nonresonant mode. We required that the real photon energy in the center-of-mass frame is at least 1% of the impinging positron energy. This cutoff value is commonly adopted in such calculations [49]. The cutoff discriminates between the "hard" regime, where Eq. (4) is applicable, and the "soft" one. The low-energy contribution to the total cross section should be reabsorbed in the resonant part, resulting in an effective enlargement of the A' width. For our specific case, the enlargement is $\simeq 20\%$. This affects the signal yield Y in the case of A' resonant production, directly proportional to the resonance width. However, as discussed in the following section, the dependence of the exclusion limit on Y is weak. This makes the correction negligible.

The main kinematic characteristics of the two annihilation mechanisms are as follows. In the case of resonant positron annihilation, the kinematics of the produced A' is strongly constrained by the one-body nature of the final state. A dark photon with mass $m_{A'}$ is produced with energy $E_R = \frac{m_{A'}^2}{2m_e}$, in the same direction of the impinging positron. For the nonresonant case, instead, the A' angular distribution in the CM frame, given by Eq. (3), is concentrated in the e^+e^- direction, due to the $1 - \beta^2 z^2$ factor at the denominator. This results in an angular distribution in the laboratory frame strongly peaked in the forward direction, the effect being more intense for larger values of the A' mass. The maximum A' emission angle in the laboratory frame is $\theta_{A'}^{\max} \simeq \frac{s - m_{A'}^2}{2m_{A'}E_0}$ (see Fig. 3). The corresponding energy distribution ranges from E_R to the primary positron energy E_0, with an average value of $\frac{E_0}{2}\left(1 + \frac{m_{A'}^2}{2m_eE_0}\right)$.

III. ELECTRON BEAM ON A THICK TARGET

In the following, we investigate the possibility of using the A' production processes by positrons previously described in an electron-beam fixed-target scenario, exploiting secondary e^+ emitted through standard electromagnetic processes. When a high-energy electron impinges on a material, it initiates an electromagnetic shower (EM), that is, a cascade multiparticle production process. The two main reactions contributing to the process are photon production through bremsstrahlung by electrons and positrons and e^+e^- pair production by photons. As a consequence, after a few radiation lengths, the developing shower is made by an admixture of electrons, positrons, and photons, characterized by different energy distributions.

In previous papers describing A' production in electron beam-dump experiments [37], only the bremsstrahlunglike
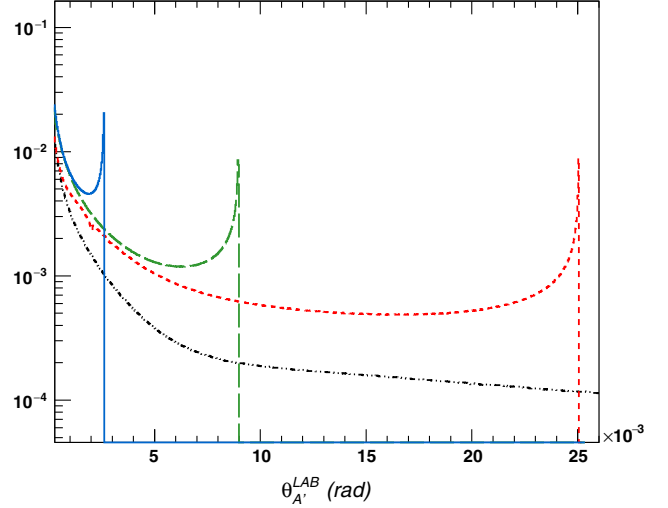

FIG. 3. The angular distribution in the laboratory frame of A' produced in nonresonant annihilation of 20-GeV positrons for different dark photon masses: 20 (red, short-dashed line), 50 (green, long-dashed line), and 100 MeV/c^2 (blue, continuous line). For comparison, the angular distribution of photons in the process $e^+e^- \to \gamma\gamma$ is also shown (black, dash-dotted line).

dark photon production by electrons has been included (we refer to Ref. [50] for a critical discussion of limitations of the widely used Weizsäcker-Williams approximation within this context). In this work, we discuss how, in the positron-rich environment produced by the high-energy electron showering in a beam dump, contributions from nonresonant and resonant annihilation can be sizable. As a rule of thumb, compared to the characteristic shape of A'-strahlung exclusion limits, the resonant annihilation process leads to a more stringent constraint at low ε, in the A' mass window constrained by the primary beam energy (right bound) and by the detection threshold (left bound).

To evaluate the A' production by positrons and the subsequent detection of the visible decay products (e^+e^- pairs) in an electron-beam dump experiment, we employed the following Monte Carlo procedure. First, we evaluated the energy spectrum and the multiplicity of secondary positrons in the beam dump through a GEANT4-based [51] simulation. Then, we used this result as input for a custom Monte Carlo code that generates A' events according to the two positron annihilation processes described above, handles the A' propagation and subsequent decay to an e^+e^- pair, and includes the experimental acceptance of a detector placed downstream of the dump. The code also computes the total number of produced particles per electron on target (EOT). We found this dual-step method more effective than including the dark photon as a new particle in GEANT4, together with the corresponding production mechanisms. Decoupling the A' production in the dump from the EM shower development allows us to handle cases with $\varepsilon \ll 1$ without generating a very large number of EM showers in the target. This is possible by artificially enhancing the A'

production cross section in the second step, properly accounting for this in the final reach evaluation. Also, this method saves computation time while evaluating the sensitivity of a beam-dump experiment as a function of the A' mass and coupling. Indeed, for a given experimental setup, the first step is performed only once, while only the second, i.e., A' generation and detector acceptance evaluation, is repeated for different dark photon masses and couplings.

A. A' production yield

The total A' yield per EOT due to positron annihilation is given by

$$N_{A'} = \frac{N_A}{A} Z\rho \int_{E_{\min}^R}^{E_0} dE_e T_+(E_e)\sigma(E_e), \qquad (5)$$

where A, Z, and ρ, are, respectively, the target material atomic mass, atomic number, and mass density, E_0 is the primary beam energy, N_A is Avogadro's number, $\sigma(E_e)$ is the energy-dependent A' production cross section, and $E_{\min}^R = \frac{m_{A'}^2}{2m_e}$ is the minimal positron energy required to produce a dark photon with mass $m_{A'}$ through positron annihilation on atomic electrons (see Sec. II). Finally, $T_+(E_e)$ is the positron differential track-length distribution. We note that the same approach applies in case of bremsstrahlunglike A' production by electrons, with $\sigma(E_e)$ replaced by the corresponding cross section and the track length being that of electrons in the dump.

Since the typical dark photon width accessible by beam-dump experiments is much smaller than the scale of T_+ variations, Eq. (5) reduces to

$$N_{A'} \simeq \frac{\pi}{2}\frac{N_A}{A} Z\rho\sigma_{\mathrm{peak}}\Gamma_{A'}\frac{m_{A'}}{m_e} T_+(E_R) \qquad (6)$$

in the case of A' resonant production.

B. Positron track-length distribution

The positron track-length distribution $T_+(E_e)$ is defined as the integral over the beam-dump volume of the differential fluence $\Phi(E_e)$, corresponding to the density of particle tracks in the volume [52]. Intuitively, the quantity $T_+(E_e)dE_e$ represents the total path length in the dump taken by positrons with energy in the interval between E_e and $E_e + dE_e$.

The differential track length can be calculated by assuming that all particles propagate along the primary beam axis, thus neglecting the transverse contribution to the path length from angular straggling. This approximation is well justified by the fact that the electromagnetic shower is strongly peaked in the forward direction so that the corresponding effects on the shape and the normalization of $T_+(E_e)$ are negligible. We underline that the longitudinal approximation is valid in the context of $T_+(E_e)$ calculation, while

angular effects in the shower have to be considered when computing the detection acceptance, as described later.

Under this hypothesis, $T_+(E_e)$ can be obtained by integrating the differential energy distribution $I_e^+(E_e, t)$ of positrons over the full beam-dump length:

$$T_+(E) = \int_0^{L_{\mathrm{dump}}} I_e^+(E_e, t)dt. \qquad (7)$$

Here, $I_e^+(E_e, t)$ is normalized so that $\int_0^{E_0} I_e^+(E_e, t)dE_e$ is the total positron current per EOT through a plane perpendicular to the beam axis, located at the depth t in the beam dump.

The GEANT4-based application we developed to evaluate $T_+(E_e)$ for a generic electron thick-target setup works as follows. The target length L_{dump} is divided in N thin layers of thickness Δt, located at t_i, and the differential positron current $I_e^+(E)$, normalized per EOT, is sampled on a plane positioned at depth t_i. The differential track length $T_+(E)$ has then been obtained by summing over the different planes and multiplying by the layer thickness:

$$T_+(E_e) = \Delta t \sum_{i=1}^{N} I_+^e(E_e, t_i). \qquad (8)$$

The values of N and Δt have to be tuned to the primary electron-beam energy and to the beam-dump characteristics. For a multi-GeV electron beam impinging on a thick ($L_{\mathrm{dump}} \gg X_0$) target, this procedure yields stable results for $\Delta t < X_0/10$ and $N > 200$. We also verified that no appreciable variations in results are found when, in the previous equation, the differential fluence $\Phi_+^e(E_e, t_i)$ of positrons sampled at the depth t_i is used, thus confirming the validity of the longitudinal approximation.

As an example, Fig. 4 shows the differential track-length distribution of positrons and electrons, for a 20-GeV electron beam impinging on an aluminum beam dump. It is worth noticing that the two distributions have different shapes at a high energy, since positrons are generated only as secondary particles in the electron-induced process. To validate the result, we also compared it with the output of a FLUKA-based simulation [53,54], where the built-in differential track-length scorer has been employed, finding an agreement at a few percent level in the full energy range. In the following, we considered this difference as the systematic error associated to $T_+(E_e)$. Since, at a fixed $M_{A'}$, limits on ε scale roughly as $(T_+)^{\frac{1}{4}}$ (lower bound) or $\log(T_+)$ (upper bound), the corresponding effect on the result is negligible.

The prediction of the analytical model of Ref. [55] is shown as a red dashed line in Fig. 4 (in the calculation, we considered contributions up to second-generation electrons and positrons). The model well reproduces the electron and positron track-length distribution in the full energy range. We also note that the model remarkably matches the shape
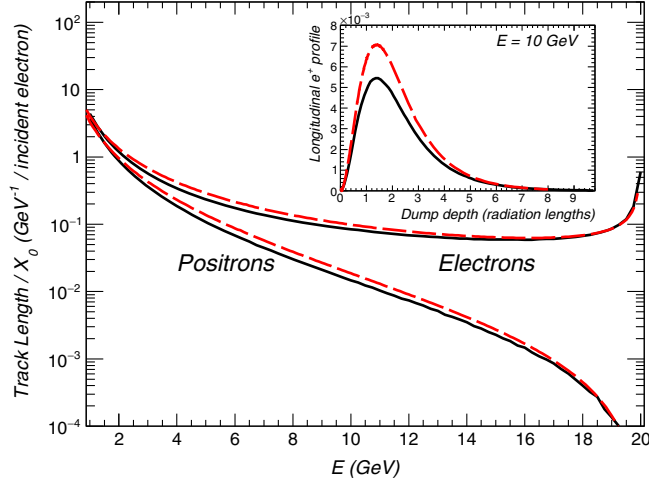
FIG. 4. Track-length distribution $T(E_e)$ for a 20-GeV electron beam impinging on an aluminum beam dump, divided by the corresponding radiation length. The red dashed line corresponds to the prediction of Tsai and Whitis [55]. The inset shows the longitudinal positron shower profile at $E_e = 10$ GeV (in GeV^{-1} per incident electron). The red dashed line corresponds to the prediction of Tsai parametrization.

FIG. 5. The rms value of the differential positrons track-length angular distribution $T_+(E_e, \vec{\Omega}_e)$, as a function of $x = E/E_0$, for different values of the primary electron-beam energy E_0: 100 (black circles), 20 (red squares), and 11 GeV (blue triangles).

of the longitudinal shower of both particles, i.e., the dependence of $I^e_\pm(E_e, t)$ as a function of the depth t for fixed positron energy E_e, describing the shower evolution in the dump. The inset in the same figure shows the specific case of $E_e = 10$ GeV positrons, with $I^+_e(E_e, t)$ normalized to the aluminum radiation length.

C. Angular effects

The angular spread of positrons in the shower has a non-negligible effect in dark photon production and detection. It induces a further widening in the A' angular distribution that sums up to the intrinsic spread due to the production mechanism and to the e^+e^- decay. The latter is characterized by an average opening angle between the two leptons $\theta^{e^+e^-}_D \simeq \frac{M_{A'}}{E_{A'}}$. This may result in a sizable fraction of particles produced out of the detector geometrical acceptance.

The double-differential positron track-length distribution $T_+(E_e, \vec{\Omega}_e)$ is required in order to account for this effect, with the momentum direction $\vec{\Omega}_e$ measured with respect to the primary beam axis. To evaluate it, we used the previously described Monte Carlo–based procedure, replacing the quantity I^e_+ in Eq. (8) with the double-differential positron current $I^e_+(E_e, \vec{\Omega}_e)$. This approach, even if approximated, is motivated by the lack in the literature of a full analytical treatment of the secondary particle angular distribution in an EM shower developing in a thick target. Moreover, common particle transport codes, such as GEANT4 and FLUKA, although containing built-in scorers to estimate the track length of a specific particle
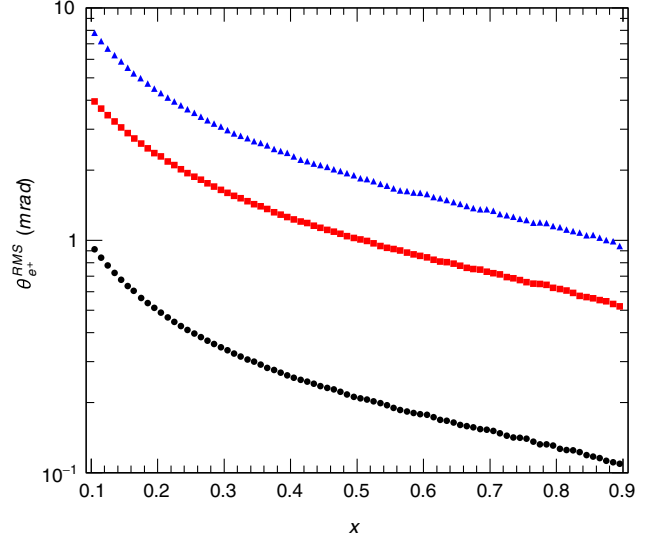
species within a volume, provide only results integrated over the full solid angle. It is worth noticing that, having the same dependence of the track-length distribution, exclusion limits are weakly affected by any uncertainty on angular distributions.

Figure 5 shows the rms value of the differential positron track-length angular distribution, as a function of $x = E_e/E_0$, for different values of the primary beam energy. The results scale approximately as $1/E_e$. This reflects the energy dependence of the two main contributions to positron angular distribution in the dump: the bremsstrahlung and pair production characteristic emission angle $\theta_1 \propto \frac{m_e}{E_e}$ and the multiple-scattering spread $\theta_2 \propto \frac{E_s}{E_e}$, with $E_s = m_e \sqrt{4\pi/\alpha} \simeq 21.2$ MeV.

A proper evaluation of angular effects is particularly critical in the case of resonant A' production. In this process, the dark photon is always produced in the positron direction. Therefore, A''s and positrons have the same angular distribution. For example, in the case of $M_{A'} = 50$ MeV/c^2 and a primary electron beam with $E_0 = 20$ GeV, dark photons, produced by positrons with energy $E_R \simeq 2.45$ GeV, would be emitted with an angular spread of about 4 mrad (see Fig. 5), comparable to the opening angle of the e^+e^- decay pair of about 20 mrad.

D. Total signal yield in the detector

A general treatment of the total signal yield in a distant on-axis detector in a beam-dump experiment searching for visible dark photon decay is reported in Ref. [37]. Here, we briefly summarize the results, explicitly including the angular dependence of the produced dark photons. Since the typical distance between the detector and the beam

dump is much larger than the length of the latter, to compute the detection acceptance, we neglect the longitudinal dependence of the A' production vertex, fixed at $t = 0$ [see Eq. (11) and related comments in the aforementioned reference].

The differential dark photon distribution per EOT reads [see Eq. (6) for target luminosity factors]

$$\frac{dN}{dE_{A'}d\vec{\Omega}_{A'}} \propto \int_{E_{\min}^R}^{E_0} dE_e \int_{4\pi} d\vec{\Omega}_e T_+(E_e, \vec{\Omega}_e)$$
$$\times \frac{d\sigma(E_e)}{d\vec{\Omega}_{A'}'} \delta(E_{A'} - f(E_e, \vec{\Omega}_{A'}')), \qquad (9)$$

where $\frac{d\sigma(E_e)}{d\vec{\Omega}_{A'}'}$ is the differential A' production cross section, $\vec{\Omega}_{A'}$ and $\vec{\Omega}_{A'}'$ are, respectively, the dark photon momentum direction in the laboratory frame and in the rotated positron frame, and $f(E_e, \vec{\Omega}_{A'}')$ is the kinematic function relating the A' energy to the impinging positron energy and to the A' emission angle.

After being produced, dark photons propagate along the direction $\vec{\Omega}_{A'}$ with a differential decay probability per unit path given by

$$\frac{dP}{dl} = \frac{1}{\lambda} e^{-l/\lambda}, \qquad (10)$$

where $\lambda = \frac{E_{A'}}{m_{A'}} \frac{1}{\Gamma_{A'}}$ is the A' decay length.

Electron and positrons from the A' decay are emitted on a cone with a typical aperture $\theta_D^{e^+e^-} \simeq \frac{M_{A'}}{E_{A'}}$ with respect to the $\vec{\Omega}_{A'}$ axis. The total signal yield is thus obtained combining the A' angular distribution [Eq. (9)] with the decay kinematics and integrating the result over the geometrical acceptance of the detector. The latter can be roughly determined as the product of a longitudinal factor ε_L depending on the shielding $L_{\rm sh}$ and decay region $L_{\rm dec}$

length and a transverse factor ε_T related to the detector face width S (see Fig. 6):

$$\varepsilon_L \simeq e^{-L_{\rm sh}/\lambda} \cdot (1 - e^{-L_{\rm dec}/\lambda}), \qquad (11)$$

$$\varepsilon_T \simeq S/(\theta_{A'}^{\rm rms}(L_{\rm sh} + L_{\rm dec}) \oplus \theta_D^{e^+e^-} L_{\rm dec}), \qquad (12)$$

with $\theta_{A'}^{\rm rms}$ being the width of the dark photon angular distribution and $\theta_D^{e^+e^-}$ the typical opening angle between the e^+e^- pair from A' decay. It is worth noticing that the above expression for ε_T holds exactly in the case of A' decay happening at the beginning of the decay volume (large ε case). In other cases, it leads to a detection acceptance underestimate, since the contribution of $\theta_D^{e^+e^-}$ to the transverse displacement is actually smaller. Given that, for typical beam-dump experiments, $L_{\rm dec} \approx L_{\rm sh}$ and that $\theta_{A'}^{\rm rms} \approx \theta_D^{e^+e^-}$, the obtained result is valid within a factor of $\simeq 2$.

To evaluate the detection acceptance, we generate a large set of A' events by randomly sampling positrons from the $T_+(E, \vec{\Omega}_e)$ distribution. For each positron, a dark photon is generated according to the production cross section. Finally, the A' is propagated along the $\vec{\Omega}_{A'}$ direction, with the e^+e^- pair generated at the decay vertex assuming an isotropic distribution in the dark photon rest frame. The detector acceptance is determined by counting the number of electrons or positrons hitting the detector. To speed up calculations, dark photons are always forced to decay in the region between the shielding and the detector. A weight ε_L is associated to each event to account for it.

IV. EXCLUSION LIMITS FROM THE E137 EXPERIMENT

In this section, we derive the contributions of resonant and nonresonant e^+ annihilation in the specific case of the SLAC E137 experiment [39]. Among the past electron
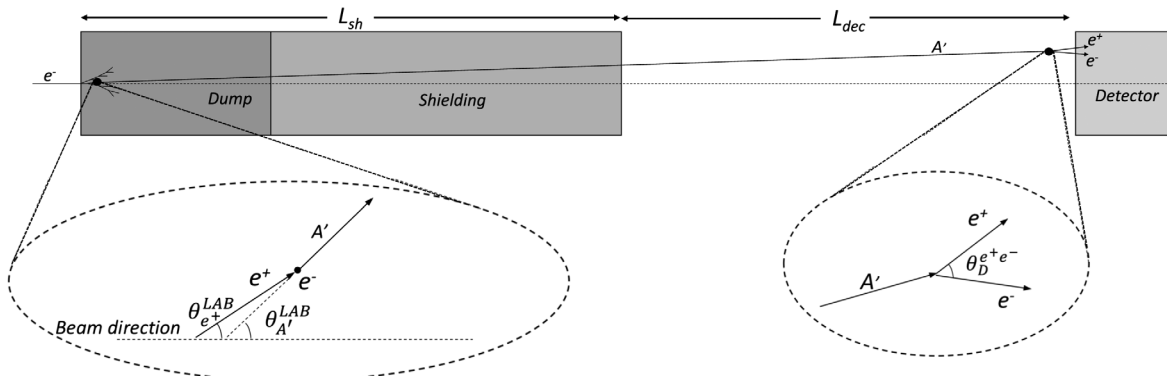

FIG. 6.   Typical setup of a beam-dump experiment for visible decay A' search. $L_{\rm sh}$ is the total length of target and shielding, while $L_{\rm dec}$ is the length of the downstream decay region, preceding the detector. The two insets show schematically the angles involved in the A' production and decay processes, as described in the text.

beam-dump experiments reanalyzed in the context of an A' search [37], E137 is the one sensitive to the smallest values of ε, down to $\simeq 10^{-8}$ (see Fig. 1). We decided to focus on this experiment, because, as shown below, the two new production mechanisms extend the exclusion limits to lower values of A' coupling with respect to the bremsstrahlunglike diagram only.

The E137 experiment searched for long-lived neutral objects produced in the electromagnetic shower initiated by 20-GeV electrons in the SLAC beam dump. Particles produced in the water-cooled aluminum plates forming the dump would have to penetrate 179 m of earth shielding and decay in the 204 m region downstream of the shield. The E137 detector consists of an 8-radiation length electromagnetic calorimeter made by a sandwich of plastic scintillator paddles and iron (or aluminum) converters. Multiwire proportional chambers provided an accurate angular resolution, essential to keep the cosmic background to a negligible level. A total charge of ~30 C was dumped during the live time of the experiment in two slightly different experimental setups: In the first run (accumulated charge $\simeq 10$ C), the detector had a transverse size of 2×3 m^2, while in the second run this was 3×3 m^2.

The original data analysis searched for axionlike particles decaying in $e^+ e^-$ pairs, requiring a deposited energy in the calorimeter larger than 1 GeV with a track pointing to the beam-dump production vertex. The absence of any signal provided stringent limits on axions and photinos. Negative results were used in Refs. [37,43] to set strong constraints on the visible decay $A' \to e^+ e^-$ assuming the A'-strahlung [Fig. 2(a)] as the only production mechanism. Including the resonant and nonresonant positron annihilation, we have derived extended and more accurate limits for the A' coupling to SM particles.

To derive the E137 exclusion limits for resonant and nonresonant A', we used the Monte Carlo–based numerical approach described above. The experimental acceptance was evaluated separately for the two E137 runs and combined with proper weights to account for the different accumulated charges. In the calculation, we employed the same selection cuts used in the original analysis:

(i) The energy of the impinging e^+/e^- particle has to be larger than 1 GeV. We note that, in the case of resonant production, this puts a hard limit on the minimum value of the A' mass of about 33 MeV/c^2.

(ii) The angle of the impinging particle on the detector, measured with respect to the primary beam axis, has to be smaller than 30 mrad.

We found that both particles from A' decay hit the detector in a non-negligible fraction of events. In these cases, we applied previous selection cuts respectively considering the sum of the two energies to be greater than 1 GeV and the energy-averaged impinging angle to be less than 30 mrad.

Based on the null observation reported by E137, we derived the exclusion contour considering a
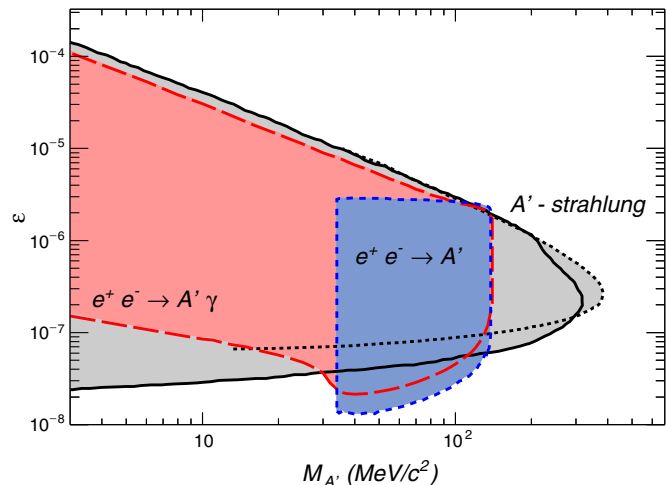

FIG. 7. Exclusion limits on the ε vs $M_{A'}$ parameter space derived from the E137 experiment considering e^+ nonresonant (long-dashed red line) and resonant (short-dashed blue line) production. Results from a previous analysis which included only production via A'-strahlung are depicted as black solid [37] and black dotted [43] lines.

95% C.L. upper limit of three events. Figure 7 shows results for both resonant (short-dashed blue line) and nonresonant (long-dashed red line) annihilation. Limits obtained by the A'-strahlung from Refs. [37,43] are shown in the figure as a black solid line and a black dotted line, respectively. Resonant annihilation provides the best exclusion limits for $m_{A'}$ in the (33 MeV/$c^2 < m_{A'} < 120$ MeV/c^2) range, strengthening by almost a factor of 2 the previous limits. The lowest limit on $\varepsilon \sim 10^{-8}$ is obtained for $m_{A'} = 33$ MeV/c^2. In the case of resonant annihilation, the sharp cutoff at a low mass is determined by the energy detection threshold. At large ε, the reach is limited by the small A' decay width, not sufficiently dilated by the Lorentz boost factor and thus resulting in the A' decay within the shielding. The nonresonant contribution is slightly less sensitive but extends the reach to lower masses down to $m_{A'} \sim$ few MeV/c^2, for ε values ranging from $O(1)$ to $O(10)$ with respect to the limit obtained by considering the A'-strahlung.

V. CONCLUSIONS

In this paper, we showed that e^+ resonant and nonresonant annihilation are two viable dark photon production mechanisms competitive with the widely considered A'-strahlung. This argument can be applied to electromagnetic showers initiated by an electron beam in a thick target. We used a Monte Carlo–based approach to numerically derive the energy and angular distribution of A' produced in a beam dump and evaluated the effect on the accepted yields on a downstream detector. We explicitly recalculated the reach of

the E137 experiment showing that, taking into account resonant and nonresonant annihilation, the exclusion limits in the $m_{A'}$ range (33 MeV/c^2–120 MeV/c^2) are pushed down by a factor of 2. This work shows that secondary positron annihilation needs to be included for a correct evaluation of all the exclusion limits obtained with electron beams.

[1] G. Arcadi, M. Dutra, P. Ghosh, M. Lindner, Y. Mambrini, M. Pierre, S. Profumo, and F. S. Queiroz, Eur. Phys. J. C **78,** 203 (2018).

[2] B. Holdom, Phys. Lett. B **166,** 196 (1986).

[3] E. Izaguirre, G. Krnjaic, P. Schuster, and N. Toro, Phys. Rev. D **88,** 114015 (2013).

[4] B. Batell, M. Pospelov, and A. Ritz, Phys. Rev. D **80,** 095024 (2009).

[5] R. Essig, J. Kaplan, P. Schuster, and N. Toro, arXiv:1004.0691.

[6] F. D. Aguila, G. Coughlan, and M. Quirs, Nucl. Phys. **B307,** 633 (1988).

[7] N. Arkani-Hamed and N. Weiner, J. High Energy Phys. 12 (2008) 104.

[8] C. Boehm and P. Fayet, Nucl. Phys. **B683,** 219 (2004).

[9] D. E. Soper, M. Spannowsky, C. J. Wallace, and T. M. P. Tait, Phys. Rev. D **90,** 115005 (2014).

[10] J. D. Bjorken, R. Essig, P. Schuster, and N. Toro, Phys. Rev. D **80,** 075018 (2009).

[11] E. Izaguirre, G. Krnjaic, P. Schuster, and N. Toro, Phys. Rev. D **91,** 094026 (2015).

[12] E. Izaguirre, G. Krnjaic, P. Schuster, and N. Toro, Phys. Rev. Lett. **115,** 251301 (2015).

[13] P. deNiverville, D. McKeen, and A. Ritz, Phys. Rev. D **86,** 035022 (2012).

[14] B. Batell, P. deNiverville, D. McKeen, M. Pospelov, and A. Ritz, Phys. Rev. D **90,** 115014 (2014).

[15] B. Batell, R. Essig, and Z. Surujon, Phys. Rev. Lett. **113,** 171802 (2014).

[16] P. deNiverville, M. Pospelov, and A. Ritz, Phys. Rev. D **84,** 075020 (2011).

[17] J. P. Lees *et al.* (*BABAR* Collaboration), Phys. Rev. Lett. **119,** 131804 (2017).

[18] J. P. Lees *et al.* (*BABAR* Collaboration), Phys. Rev. Lett. **113,** 201801 (2014).

[19] D. Babusci *et al.* (KLOE Collaboration), Phys. Lett. B **720,** 111 (2013).

[20] P. Adlarson *et al.* (WASA-at-COSY Collaboration), Phys. Lett. B **726,** 187 (2013).

[21] H. Merkel *et al.* (A1 Collaboration), Phys. Rev. Lett. **106,** 251802 (2011).

[22] S. Abrahamyan *et al.* (APEX Collaboration), Phys. Rev. Lett. **107,** 191804 (2011).

[23] R. Corliss (DarkLight Collaboration), Nucl. Instrum. Methods Phys. Res., Sect. A **865,** 125 (2017).

[24] A. Celentano (HPS Collaboration), J. Phys. Conf. Ser. **556,** 012064 (2014).

[25] M. Raggi and V. Kozhuharov, Adv. High Energy Phys. **2014,** 1 (2014).

[26] B. Wojtsekhowski, G. Baranov, M. Blinov, E. Levichev, S. Mishnev, D. Nikolenko, I. Rachek, Y. Shestakov, Y. Tikhonov, D. Toporkov, J. Alexander, M. Battaglieri, A. Celentano, R. D. Vita, L. Marsicano, M. Bondí, M. D. Napoli, A. Italiano, E. Leonora, and N. Randazzo, J. Instrum. **13,** P02021 (2018).

[27] J. L. Feng, B. Fornal, I. Galon, S. Gardner, J. Smolinsky, T. M. P. Tait, and P. Tanedo, Phys. Rev. Lett. **117,** 071803 (2016).

[28] J. Alexander, Eur. Phys. J. Web Conf. **142,** 01001 (2017).

[29] A. A. Aguilar-Arevalo *et al.* (MiniBooNE-DM Collaboration), Phys. Rev. Lett. **118,** 221803 (2017).

[30] M. Bondí (BDX Collaboration), Eur. Phys. J. Web Conf. **142,** 01005 (2017).

[31] J. Mans (LDMX Collaboration), Eur. Phys. J. Web Conf. **142,** 01020 (2017).

[32] E. Izaguirre, G. Krnjaic, and M. Pospelov, Phys. Rev. D **92,** 095014 (2015).

[33] Y. Kahn, G. Krnjaic, J. Thaler, and M. Toups, Phys. Rev. D **91,** 055006 (2015).

[34] D. Banerjee *et al.* (NA64 Collaboration), Phys. Rev. Lett. **118,** 011802 (2017).

[35] J. Alexander *et al.*, arXiv:1608.08632.

[36] M. Battaglieri *et al.*, arXiv:1707.04591.

[37] S. Andreas, C. Niebuhr, and A. Ringwald, Phys. Rev. D **86,** 095019 (2012).

[38] E. M. Riordan *et al.*, Phys. Rev. Lett. **59,** 755 (1987).

[39] J. D. Bjorken, S. Ecklund, W. R. Nelson, A. Abashian, C. Church, B. Lu, L. W. Mo, T. A. Nunamaker, and P. Rassmann, Phys. Rev. D **38,** 3375 (1988).

[40] A. Bross, M. Crisler, S. Pordes, J. Volk, S. Errede, and J. Wrbanek, Phys. Rev. Lett. **67,** 2942 (1991).

[41] A. Konaka *et al.*, Phys. Rev. Lett. **57,** 659 (1986).

[42] M. Davier and H. N. Ngoc, Phys. Lett. B **229,** 150 (1989).

[43] Y.-S. Liu and G. A. Miller, Phys. Rev. D **96,** 016004 (2017).

[44] E. Nardi, in *New Directions in Dark Matter and Neutrino Physics* (Perimeter Institute, Waterloo, Canada, 2017), PI Video Library: http://pirsa.org/17070015.

[45] E. Nardi, C. D. R. Carvajal, A. Ghoshal, D. Meloni, and M. Raggi, Phys. Rev. D **97,** 095004 (2018).

[46] A. J. Krasznahorkay *et al.*, Phys. Rev. Lett. **116,** 042501 (2016).

[47] Y.-S. Tsai, Rev. Mod. Phys. **46**, 815 (1974); **49**, 421 (1977).

[48] C. Patrignani *et al.* (Particle Data Group), Chin. Phys. C **40**, 100001 (2016).

[49] M. Bohm and W. Hollik, Phys. Lett. **139B**, 213 (1984).

[50] Y.-S. Liu, D. McKeen, and G. A. Miller, Phys. Rev. D **95**, 036010 (2017).

[51] S. Agostinelli *et al.*, Nucl. Instrum. Methods Phys. Res., Sect. A **506**, 250 (2003).

[52] A. Chilton, Health Phys. **34**, 715 (1978).

[53] T. Bhlen, F. Cerutti, M. Chin, A. Fassó, A. Ferrari, P. Ortega, A. Mairani, P. Sala, G. Smirnov, and V. Vlachoudis, Nucl. Data Sheets **120**, 211 (2014).

[54] A. Ferrari, P. R. Sala, A. Fasso, and J. Ranft, Technical Report No. CERN-2005-010, SLAC-R-773, INFN-TC-05-11, 2005.

[55] Y. S. Tsai and V. Whitis, Phys. Rev. **149**, 1248 (1966).